THE JOURNAL OF PHYSICAL CHEMISTRY C

Article

pubs.acs.org/JPCC

Water Film Adsorbed on the α-Al_2O_3(0001) Surface: Structural Properties and Dynamical Behaviors from First-Principles Molecular Dynamics Simulations

Shang-Yi Ma,[†] Li-Ming Liu,*[,‡,§] and Shao-Qing Wang[†]

[†]Shenyang National Laboratory for Materials Science, Institute of Metal Research, Chinese Academy of Sciences, Shenyang 110016, China

[‡]Beijing Computational Science Research Center, Chinese Academy of Engineering Physics, Beijing 100084, China

[§]Chengdu Green Energy and Green Manufacturing Technology R&D Center, Chengdu 610207, China

ABSTRACT: We investigated the structural properties, dynamical behaviors, and vibrational spectra of the water film adsorbed on the Al-terminated α-Al_2O_3(0001) surface using first-principles molecular dynamics simulations. The simulations showed that the structural properties of the water film, such as the mass density, atom number density, orientation order and hydrogen bonds (HBs) of water molecules, are considerably affected by the Al-terminated α-Al_2O_3(0001) surface along its normal direction. A new dissociation 1−4′ state via two different indirect and double indirect pathways was proposed, which is slightly more favorable than 1−4 state under the condition of multiple water layers. The blue- and red-shifting of vibrational spectra for different water layers was observed. The interfacial water in various adsorption configurations and its corresponding vibrational spectrum were explicitly identified. The "ice-like" and "liquid-like" peaks of vibrational spectra, which are observed in various experiments of water/hydroxylated α-Al_2O_3(0001) interface, were reproduced in our simulations. Our simulations suggest the "ice-like" peak mostly stems from the surface OH and the interfacial water molecules that experienced more HBs interactions, while the "liquid-like" peak results from the "liquid-like" water molecules. Our study provides novel insights into the complex structures and dynamical behaviors of interfacial water, upon water film adsorbing on the Al-terminated α-Al_2O_3(0001) surface.

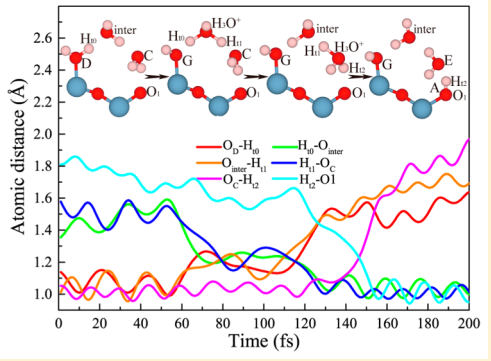

INTRODUCTION

The ubiquitous presence of water on surfaces at ambient conditions means that water/solid interfaces are relevant to an incredibly broad range of physicochemical phenomena and scientific and technological processes such as corrosion, lubrication, heterogeneous catalysis and electrochemistry. In the past few years, tremendous progresses in a fundamental understanding of water at metal surfaces were attained with well-defined studies at the molecular level.[1−3] However, an understanding of water adsorption on metal oxides surfaces lagged behind due to the additional complexity of metal oxides. The Al_2O_3(0001) surface is among the metal oxide surfaces that have received particular experimental and theoretical interests due to its broad scientific and technological importance in areas such as catalysis, microelectronics and nanoelectronics, ceramics, geochemical, and environmental chemistry.[4,5]

Experimental studies of single water adsorption on a clean and stable surface were generally carried out under ultrahigh vacuum (UHV) conditions. Under UHV conditions, the Al-terminated α-Al_2O_3(0001) has been experimentally[6−8] and theoretically[9,10] demonstrated to be the most stable surface, in which instance only the molecular adsorption and desorption of H_2O is observed at nondefect α-Al_2O_3(0001) surface at or below 300 K (<10^{-8} Torr).[11−13] The formation of surface OH is observed only at a pressure above ∼1 Torr and 300 K with X-ray photoelectron spectroscopy (XPS),[11] laser-induced thermal desorption (LITD), and temperature-programmed desorption (TPD) measurements.[12] Once created, isolated surface OH groups are quite stable on an alumina surface under UHV conditions.[14] The hydroxyl-free α-Al_2O_3(0001) surface is hard to obtain even after annealing at ∼1400 K.[6] Theoretically, density functional theory (DFT) and supercell slab mode study indicated that a single H_2O molecule exclusively adsorbs to the Lewis acidic Al site of the α-Al_2O_3(0001) surface through an O atom, with an adsorption energy of −1.14 eV.[15] Further calculations found that dissociation adsorption rather than molecular adsorption is more favorable in energy, and molecularly adsorbed water can dissociate readily even in the absence of defects.[15−18] Two competing dissociation states, 1−2 and 1−4 states, have been proposed, which correspond to the states that the preadsorbed H_2O splitting into H^+ and OH^-, and then the proton H^+ transferring to the nearest and the

Received: November 2, 2015
Revised: February 22, 2016
Published: February 22, 2016

DOI: 10.1021/acs.jpcc.5b10695
J. Phys. Chem. C 2016, 120, 5398−5409

second nearest O site, respectively (the 1−2 and 1−4 sites can be referred the inset shown in Figure 5).[16] Despite the fact that the 1−4 state is less stable than 1−2 state about 0.27 eV in adsorption energy,[15,19] the dissociation pathway of the 1−4 state is strongly favored over that of the 1−2 state. The dissociation barrier to the 1−4 state is estimated to be ∼0.1 eV,[16,20] while the barrier to the 1−2 state was estimated to be ∼0.29,[16] ∼ 0.15,[20] and ∼0.19 eV[19] by a variety of studies at lower coverage. By combining sum-frequency generation spectroscopy (SFGS) method and DFT calculation, the two dissociation channels have been confirmed in a very recent study.[21] With increasing water coverage, the adsorption energy per water molecule on the α-Al_2O_3(0001) surface slightly decreased.[15,17] Two adsorption modes, with the hexagonal layer consisting of molecular and dissociation adsorption water vs complete molecular adsorption water, were theoretically proposed for monolayer (ML) coverage.[15,17]

The limitation of experimental studies under UHV condition is that many important natural and industrial processes do not occur under such rarefied conditions. Surface reaction involving two or more H_2O molecules cannot be observed under UHV conditions except at low temperatures where the chemical reaction is kinetically hindered. Under ambient condition, the XPS study reported that the first monolayer is completed at ∼15% relative humidity (RH) on the α-Al_2O_3(0001) surface and followed by a second layer at 35−40% RH.[22] The XPS results showed that the surface oxygen layer is comprised of OH groups when the Al-terminated surface was exposed to ambient pressures of water vapor and subsequently transferred back to UHV.[11] At higher water exposures, the α-Al_2O_3(0001) surface was found to be hydroxyl-terminated using crystal truncation rod diffraction (CTRD), which can be rationalized as the top layer of Al being liberated mediated by multiple water dissociation and leaving behind a hydroxyl-covered surface.[7] These results are also consistent with general DFT calculations that the fully hydroxylated surface becomes more stable in the presence of H_2O.[10,17] Furthermore, the DFT static calculations showed that the water dissociation at a singly hydroxylated top Al, steps necessary to liberate top Al and reach the fully hydroxylated surface, are very complex and the barriers of which stepwise increase with the increasing hydroxyl coverage.[19] It is also experimentally reported that the surface hydroxylation is H_2O pressure dependent.[11] Therefore, there are qualitative differences on the H_2O/α-Al_2O_3(0001) surface interactions under ambient and UHV condition. Detailed information regarding the dynamical behavior of surface hydroxylation is still scant.

Under ambient condition, the thickness of water film absorbed on the α-Al_2O_3(0001) surface grows with increasing RH, and three water layers are completed at living environment (55% RH).[22] The first contacting layer, which is highly related to surface reactivity, is intensively examined in experiments with various methods.[22−31] However, comparisons between various measurements are more or less complicated by the difficulty in preparing clean and well-defined surface termination, which make it difficult to test specific assignments of the closely spaced OH peaks observed in experiments. The vibrational spectra of interfacial water obtained with the sum-frequency generation spectroscopy (SFGS) and sum-frequency vibrational spectroscopy (SFVS) are pH dependent and composed of multiple broad, overlapping bands, rendering their interpretation more difficult. The band at ∼3430 cm^{-1} commonly observed in the vibrational spectrum of interfacial water was assigned to the OH stretching of adsorbed water in the study of Al-Abadleh and Grassian,[23] while it was assigned to the OH groups protruding from the surface.[32] Two distinct broad bands, the "ice-like" at ∼3200 cm^{-1} and the "liquid-like" at ∼3450 cm^{-1} are commonly found in a variety of spectrum experiments of water/solid interface.[23,26−28,31−34] However, the interpretation on these two bands is still debatable. Sung et al. assigned the former and latter peaks to the interfacial water molecules and the surface OH group, respectively.[27] Alternatively, Ostroverkhov et al. proposed that the former peak represents OH in a more ordered ice-like hydrogen-bonding network, and the latter one in a less ordered liquid-like hydrogen-bonding structure.[33] Whereas, Sovageo et al. suggested that the double peaks originate from vibrational coupling between the stretching and bending overtone rather than from the existence of distinct water substructures.[28] Additionally, it is hard to directly probe thicker water layers in experiments in detail, thereby it cannot afford molecular information about the structures and dynamical behaviors of the buried interfacial water. Very recently, these questions beyond experiments are accessed with theoretical methods, such as the empirical MD simulations,[35,36] FPMD simulations,[37] DFT calculations, and Monte Carlo (MC) simulations.[38] However, these studies, more or less, are limited by inaccuracy description of interatomic interactions and short time of dynamical simulations.

Though the Al-terminated α-Al_2O_3(0001) surface is well-known to become hydroxylated in the presence of water, the hydroxylation process cannot complete instantaneously and many interesting water dissociation steps are involved. The present work stems from the necessity of a better understanding of the complex structures of interfacial water and the dynamical behaviors occurring at the initial stage of surface hydroxylation, upon nanoscale water film adsorbing on Al-terminated α-Al_2O_3(0001) surface. The water molecules in different adsorption configurations were identified in our calculations. A new 1−4′ dissociation state through the indirect and double indirect water dissociation pathways was proposed. Furthermore, we calculated the vibrational spectra of waters in various configurations, which provide further interpretation on the experimental data and on the "ice-like" and "liquid-like" spectrum shoulders observed in experiments.

CALCULATION METHODS AND SIMULATION MODEL

The structure and dynamical behaviors of the water film adsorbed on Al-terminated α-Al_2O_3(0001) surface were explored within the framework of DFT using the Gaussian and plane wave (GPW) approach, as implemented in the CP2K/Quickstep package.[39] The electron exchange and correlation were described with the generalized gradient approximation of Perdew−Burke−Ernzerhof (PBE) functional,[40] along with the norm-conserve Goedecker-Teter-Hutter pseudopotentials.[41−43] The wave functions of the valence electrons were expanded in terms of Gaussian functions with double-ζ valence and single polarized basis set (DZVP) for H, O, and Al atoms. For the auxiliary plane wave expansion of the charge density, the energy cutoff was set to 320 Ry. The optimizer of orbital transformations was used for the solution of the self-consistent field (SCF) equations. The strict convergence criteria of 1.0^{-7} Ha was used for the SCF calculations, in which instance the drift of the total energy is lower than 1.0^{-6} Ha/ps per atom during the whole simulations. The initial

DOI: 10.1021/acs.jpcc.5b10695
J. Phys. Chem. C 2016, 120, 5398−5409

structure of water film was obtained from an equilibrated simulation performed with empirical potentials. Then the water film was placed on the α-Al_2O_3(0001) surface and the Born−Oppenheimer molecular dynamic (BOMD) simulation up to 63 ps was performed within the canonical ensemble (NVT). The artificial substitution of deuterium (D) for H was used to maximize the allowable MD time step of 1 fs. We set a higher target temperature of 360 K for the NVT simulation to avoid the problem of low diffusion coefficients produced by DFT-PBE water.[44−46] The target temperature was controlled by Nose-Hoover chain thermostat. Most data collection and analysis were performed for the last 30 ps of the simulation.

The bulk α-Al_2O_3 can be described in terms of alternating O and Al atom layers in the sequence of ···Al−O_3−Al−Al-O_3-Al··· along the [0001] direction. The 12 Al layers approximately follow the fcc-type stacking, while the six O layers follow the hcp-type stacking. The structures and the dynamical behaviors of water film on the nonpolar Al-terminated α-Al_2O_3(0001) surface (Al_s-O_s-Al- termination, here Al_s and O_s atoms refer to the surface Al atoms and the subsurface O atoms, resepctively) were considered in the following simulation. The stoichiometric α-Al_2O_3(0001) surface was laterally modeled by 3 × 3 hexagonal surface cells, with 14.418 Å on a side. The DFT calculation performed by Ranea et al.[15] indicated that the surface energy of Al-terminated α-Al_2O_3(0001) surface is well converged beyond the relaxation of the topmost five layers and the displacements of ions from their ideal positions are less than 1% beyond the relaxation of seven layers. Therefore, we considered a slab modeled by a 12-layer-thick layers (8 Al and 4 O layers), the nine upper-most layers of which were allowed to relax freely while the remaining three bottom-most layers were kept fixed in their ideal positions during the simulation. The H_2O/α-Al_2O_3(0001) system consisted of 110 H_2O molecules, 72 Al and 108 O atoms, creating a nanoscale water film of thickness up to ∼25 Å. An empty region of 15 Å along the [0001] direction was used to separate the water film and the periodic image of the alumina substrate. This large size of the slab model and the strongly insulating nature of α-Al_2O_3 enable us to use Brillouin zone sampling of Γ point without significant loss of accuracy.

RESULTS AND DISCUSSIONS

A. Interlayer Relaxation. The pronounced interlayer relaxations of the substrate were observed at the beginning of the simulation, as shown in Figure 1. It is shown that the outmost Al atoms (denoted as Al1 hereafter) significantly relaxed inward (within initial 1 ps), even descended below the subsurface O plane (denoted as O1 hereafter), and then about two-thirds of the Al1 atoms slightly restored and ended up almost coplanar with the O1 plane finally, leaving the rest Al1 atoms situating at the sites below the O1 plane. This dramatic adsorbate-induced restructuring of the Al1 layer can be observed directly from the side snapshot shown in Figure 4c. The opposite deviations of Al3 and Al6 atoms can also be noticed in Figure 1. The O atoms did not displace much and slightly vibrated at their ideal positions, which are very different from the obvious displacements of Al atoms. The interlayer contraction of Al1−O1 and Al3−Al2 induced by the deviations of Al1 and Al3 are ∼77% and ∼45%, respectively. The similar interlayer relaxations of clean α-Al_2O_3(0001) surface were also reported in previous works.[6,8−10] The contractions of ∼63%[6] and ∼53%[8] for the first interlayer (Al1−O1) were reported in experiments, while the values of ∼85%[9] and ∼86%[10] were also

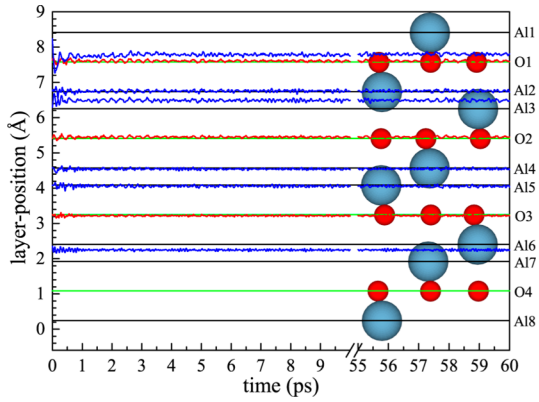

Figure 1. Interlayer relaxations of α-Al_2O_3 substrate along the [0001] direction. The substrate consists of 8 Al layers and 4 O layers in their ideal positions, in which Al and O atoms are denoted as navy and large balls, red and small balls, respectively. The black (green) lines indicate the ideal positions of Al (O) layers, while the blue (red) lines indicate the position variation of Al (O) layers during the simulation. The Al7, Al8, and O4 layers are fixed in their ideal positions during the simulation, while the other layers are free of constraints.

obtained with first-principles calculations. Furthermore, Wang et al.[10] theoretically reported that H adsorption on the Al-terminated α-Al_2O_3(0001) surface can reduce the contraction of the first interlayer spacing, from 86% to 69%. Therefore, they inferred that the measurements were affected by the surface H which is hardly eliminated from the real exposed surface. In our calculations, the contraction of the first interlayer is close to the average value of the clean and the H-adsorbed α-Al_2O_3(0001) surface, which may be the combined effects resulting from the reduced coordination of Al1 and the presence of water film. The ∼45% interlayer contraction of Al3−Al2 is well consistent with the previous calculations of ∼44%[9] and ∼49%.[10] The slight interlayer expansion was observed for Al3−O2 layer, the value of ∼23% is also consistent with other calculations of ∼20%[9] and ∼22%.[10] Additionally, the interlayer spacing of the middle layers Al4−Al5 is nearly invariable, while the interlayer contraction of the Al6−Al7 layers is up to ∼33%. This contraction might be induced by the inconsistent relaxation scheme that the three bottom atomic layers (Al7, Al8, and O4) were fixed while the Al6 layer was free of constraint, and by the presence of the water film in our simulations, since the calculations of Ranea et al.[15] demonstrated that layer relaxation is well converged within the topmost five layers.

B. Density Profile of the Adsorbed Water Film. Our simulations showed that the structure of the adsorbed water film is considerably affected by the Al-terminated α-Al_2O_3(0001) surface. The density profile of the adsorbed water film oscillates strongly along the normal direction of surface (z axis) and is highly associated with the distance from the surface (Al1-layer). The planar-average density profiles depicted in Figure 2a,b were obtained by averaging the water molecule mass and atom number with 0.1 Å interval along the z axis, respectively. Our test showed that these density profiles are insensitive to the interval width. To facilitate the following discussions, we divided the adsorbed water film into six distinct water layers according to the oscillation of its mass density profile, with the boundary being placed at the local minima point of the profile, except for the boundary between the layer V and VI. The boundary of layer V and VI was located at the point that the profile begins to incline to zero as approaching

DOI: 10.1021/acs.jpcc.5b10695
J. Phys. Chem. C 2016, 120, 5398−5409

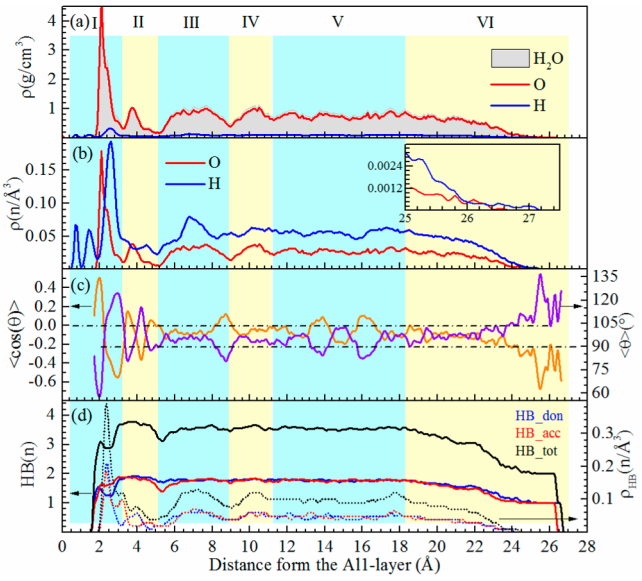

Figure 2. Structure variations of the adsorbed water film along the normal direction of surface: (a) the planar-average mass density profile of water molecules, O and H atoms; (b) the planar-average atom number density profile of O and H atoms; (c) the planar-average average orientation order parameter, $\langle\cos(\theta)\rangle$ and $\langle\theta\rangle$; (d) the total number of hydrogen bonds (HB_tot, black), the number of donor (HB_don, blue) and acceptor (HB_acc, red) per water molecule, and the planar-average density profile of hydrogen bonds. The water film was divided into six distinct layers based on the variations of mass density profile.

the vacuum. According to this divisions, the first and the last water layers include the interface of H_2O/α-$Al_2O_3(0001)$ and water/vacuum, respectively.

One can note that the water mass density of the layer I is maximally up to ~4.30 g/cm^3 (the H atomic mass is used here) at the position of ~2.10 Å, which is more than four times the density of bulk liquid water. The higher peak indicates a dense structure of water sublayer contacting the Al-terminated α-$Al_2O_3(0001)$ surface. However, the mass density of the water film steeply drops to ~0.39 g/cm^3 at the position of ~3.25 Å, which was just the boundary of water layer I and II. A minor peak, the mass density of which is about 1.0 g/cm^3, can be observed in water layer II. Then the mass density decreases to the lowest point of 0.21 g/cm^3 at the position of ~5.05 Å (the boundary of water layer II and III). The similar small valleys can also be noticed at the boundaries of layer III and IV and of layer IV and V. It is naturally inferred that these valleys stem from the depletion of water molecules in these zones. And these depleted water molecules led to the formation of the four peculiar water layers, layer I, II, III, and IV. As the distance increasing, the mass density profile becomes even and nearly approaches to the bulk liquid water density of 1.0 g/cm^3 in layer V, beyond the distance of 11.30 Å. In layer VI, the mass density stepwise inclines to zero at the water/vacuum interface. The similar higher density peak positioned at ~1.9 Å was also noticed in previous empirical MD simulations of interfacial water at the Al-terminated α-$Al_2O_3(0001)$ surface.[30,35,36] In their study, two noticeable density peaks corresponding to the formation of the water layers (hydration layer) were observed, which are slightly different from our simulations of four peculiar water layers, and these differences would be discussed in section D in detail. Experimentally, the similar and less dense layer of adsorbed water on the hydroxylated α-$Al_2O_3(0001)$ surface was also reported, obtained with specular X-ray reflectivity and atomic force spectroscopic (AFS) data.[30,36,47] The similar oscillation behaviors have also been theoretically demonstrated for the adsorbed water film on other NaCl(001),[48,49] on $TiO_2(110)$[50] and on $ZnO(10\bar{1}0)$ surface.[51]

The atom number densities were further examined to show the distribution of O and H atoms within the adsorbed water film, as shown in Figure 2(b). The H number density profile displays three pronounced peaks in layer I. The first peak at ~0.75 Å arises mainly from the surface OH produced by water dissociation, as will be discussed in sections E and F. Considering the first interlayer spacing of ~0.19 Å, the bond length of OH is ~0.94 Å. The second and the third peaks appear at the positions of ~1.45 and ~2.60 Å, respectively. By comparing the second H peak positioned at ~1.45 Å with the O peak, one may infer that there are minority water molecules contacting the surface with downward OH group. Similarly, the position of the third H peak indicates that major waters prefer to be in the orientation of the OH group pointing away from the surface. As indicated by the mass density profile of water film, the O depletion of atom number density is expected at the boundary zone between the water layers I and II and between the layer II and III. One can also note that the H number density profile extends ~0.5 Å beyond that of O at water/vacuum interface, as shown in the inset of Figure 2b, indicating a very few molecules at this interface experience the orientation of OH groups pointing toward vacuum. The similar atom number density oscillations of O and H were also observed in the empirical MD simulations of adsorbed water film on Al-terminated α-$Al_2O_3(0001)$ surface.[35] However, only two distinct H density peaks were observed in the empirical MD simulations,[35] in which study the first peak at the position of ~0.95 Å was assigned to the water molecules in OH-downward orientation, and the second one at the position of ~2.15 Å was assigned to the water molecules tending to maintain the OH group parallel and slightly pointing away from the surface. The surface hydroxyl was not considered due to the limitations of rigid water model used in this empirical MD simulation.

C. Orientation Order Parameter of the Water Molecules. A more explicit structure of the adsorbed water film can be identified by the orientation order parameter of the water molecule, θ, which is defined as the angle between the water molecule dipole and the z axis. In Figure 2c, we illustrated the planar-average $\cos(\theta)$ and θ of the water molecules as a function of O distance from Al1 layer. It can be found that though the second peak of H number density profile shown in Figure 2b suggests that there are a few water molecules tending to be in OH-downward orientation or at least one OH group of them point toward the surface, the positive peak of $\cos(\theta)$ positioned at ~2.0 Å indicates that the water molecules in OH-upward are predominant in the sublayer from ~1.7 to ~2.2 Å, with the average θ of ~56–86°. One can note that the $\cos(\theta)$ sharply turns into a negative value at the position of ~2.2 Å. The subsequent valley of $\cos(\theta)$ positioned at ~2.9 Å indicates that more water molecules prefer to be in OH-downward orientation in this region, with the average θ of ~101–124°. The change of the water dipole orientation indicates that the water layer I mainly consists of two types of water with opposite dipole orientation. These water molecules being in OH-upward and OH-downward orientations produce the well-defined and higher density of water sublayer. In layer II, one can see that the water molecules

DOI: 10.1021/acs.jpcc.5b10695
J. Phys. Chem. C 2016, 120, 5398–5409

in slight OH-downward orientations are more favored, with the average θ of ~95−117°. The slight inversion of the water dipole orientation can be noticed not only at the boundary of layer I and II but also at the boundary of II and III and III and IV. In the interior of the adsorbed water film, including layer III, IV, V, and the major part of layer VI, the average $\cos(\theta)$ fluctuates around zero point, which indicates the nearly isotropic water dipole orientation as liquid water. The fluctuation of $\cos(\theta)$ becomes sharp as it approaches the water/vacuum interface, which is highly related to the sparse distribution of water molecules in this region. The average θ of water molecules at this region is in the range of ~100−140°, which implies the water molecules being in OH-downward orientation are predominant at the water/vacuum interface.

D. Network of Hydrogen Bonds. Various properties of water are highly related to its network of hydrogen bonds (HBs). In Figure 2d, we showed the planar-average HBs of per water molecule and the HBs density profiles functioned with the distance from the Al1-layer. The common distance-angle geometric definition of the HBs proposed by Luzar and Chandler was adopted to determine the formation of HBs between water molecules in our calculations, in which definition, two water molecules are considered to be hydrogen-bonded only if their interoxygen distance is less than 3.5 Å and the angle of O−H···O is less than 30° simultaneously, and the HBs value of 3.84/water was predicted in bulk liquid PBE water.[52,53] The midposition between the donor H and the acceptor O of the two HB-bonded water molecules was defined as position of one HB. As illustrated in Figure 2d, the HBs number of per water molecule is close to that of the bulk liquid water within layers IV and V, while a distinct difference at the interfaces of water/vacuum and of H_2O/α-$Al_2O_3(0001)$ can be noticed. The HBs number of per water drops to ~2.0 as the decreasing of water mass density within layer VI, which indicates that the water molecules are undercoordinated in this region. In the nearby region of the H_2O/α-$Al_2O_3(0001)$ interface, the HBs number of per water is ~3.0, indicating the water molecules within the contacting layer possessing a fraction of broken HBs. On the whole, the number of donor and acceptor tended to be the same, small disparities can be noticed within layer I and at the boundary of layer II and III, where the acceptors and donors are slightly predominant, respectively.

Though the hydration layers within the adsorbed water film can be traced from the mass density profile of the water film, it can be examined in detail via the planar-average density profile of HBs, as shown in Figure 2d. One can note that the HBs number of per water molecule in the contacting layer is lower than that of bulk liquid water, but a pronounced peak of HBs density profile appeared in this region. The pronounced peak is just responsible for the first hydration layer of adsorbed water film, which is a very dense and highly ordered structure. The first hydration layer is at the position of ~2.4 Å, then two small bumps and a valley sequentially follow. According to the density profile of total HBs, another two weak and broad hydration layers centered at ~7.0 and ~10.3 Å can be identified, respectively. Additionally, the weaker hydration layer which is not identified by total HBs can be found at the position of ~4 Å based on the density profile of donor HBs, the peak of which corresponds with the small peak of mass density profile shown in Figure 2a. This weaker hydration layer interacts with the first dense hydration layer via acceptors, as indicated by the small peak of acceptors density profile between layer I and II. Therefore, four peculiar hydration layers, layer I, II, III, and IV, were identified at the position of ~2.4, ~ 4.0, ~7.0, and ~10.3 Å, respectively, in our FPMD simulations. In the empirical MD simulations of water film adsorbed on Al-terminated α-$Al_2O_3(0001)$ surface, though three peaks of total HBs density profile can be found at the position of ~2.1, ~2.8, and ~4.8 Å, only two hydration layers centered at ~1.90 and ~4.5 Å were identified.[35] Under the hydroxylated surface condition, three hydration layers of the adsorbed water film were reported in experimental studies.[30,47] The first and the second weak hydration layers were measured at the position of ~2.6[30] and ~2.5 Å[47], and of ~5.7[30] and ~5.6 Å[47] from the substrate, respectively. The third, much weaker hydration layer was barely observed at the position of ~9.2 Å from the substrate in AFS measurement.[30] These results indicated that the structure of interfacial water is closely related to the surface chemical conditions

In addition, the density profile of donor HBs shown in Figure 2d is lower than that of acceptor HBs at the boundary between layer I and II, which is consistent with the variation of orientation order parameter. In this instance, more acceptor over donor HBs are formed at the boundary of layer I and II because the OH-downward water molecules are predominant in this region. Thereby, the main interactions between layer I and II are acceptor HBs. The lower density profile of HBs at the boundary of layer II and III, and of and layer III and IV indicates that there are less water interactions between the layer II and III, and between layer III and IV, which may result from the presence of the Al-terminated α-$Al_2O_3(0001)$ surface.

E. Interfacial Structure of H_2O/α-$Al_2O_3(0001)$. The interfacial structure of H_2O/α-$Al_2O_3(0001)$ was examined in detail to uncover how water molecules dynamically interact with the Al-terminated α-$Al_2O_3(0001)$ surface. Water molecules involved in this interaction are mostly confined in the contacting water layer I. The contacting water layer I can be decomposed into three distinguishing sublayers according to the three distinct peaks of H number density profile. The first minor peak positioned at ~0.75 Å results from the dissociated H atoms. These dissociated H atoms adsorbed atop the O1 sites and formed the surface hydroxyl OH, as shown in Figure 3a (these OH groups were denoted as *A*-type OH hereafter). On ensemble average, there are ~3.38 A-type OH per surface, the main bond length and the deviation angle α of which are ~0.97 Å and ~73°, respectively. In Figure 3a, the angle α was defined to describe the deviation of the specific atom from the precise site. A more direct view of these dissociated and adsorbed H atoms can be approached by projecting its ensemble average spatial distribution on the surface, as the denotations of A1, A2, A3, and A4 depicted in Figure 4a. One can find that these H atoms are confined atop O1 sites in most simulation times, based on their spatial projection distributions.

The second peak of the H number density profile shown in Figure 2b results from the downward OH groups of the water molecules pointing to the O1 sites. The spatial projection distributions of these H atoms are illustrated and denoted by the letter B (B1, B2, B3, and B4) in Figure 4a, while the water molecules having these downward OH groups are denoted as C-type water molecules in Figure 3b. It is seen that the H−O1 distance and its deviation angle α are much dispersive, which mostly are in the range of ~1.5−2.2 Å and of ~50−90°, respectively. These dispersive characters of H−O1 indicate the fluctuating and swinging motion of the C-type water molecules. One OH group of C-type water points to the O1 sites with the

DOI: 10.1021/acs.jpcc.5b10695
J. Phys. Chem. C 2016, 120, 5398−5409

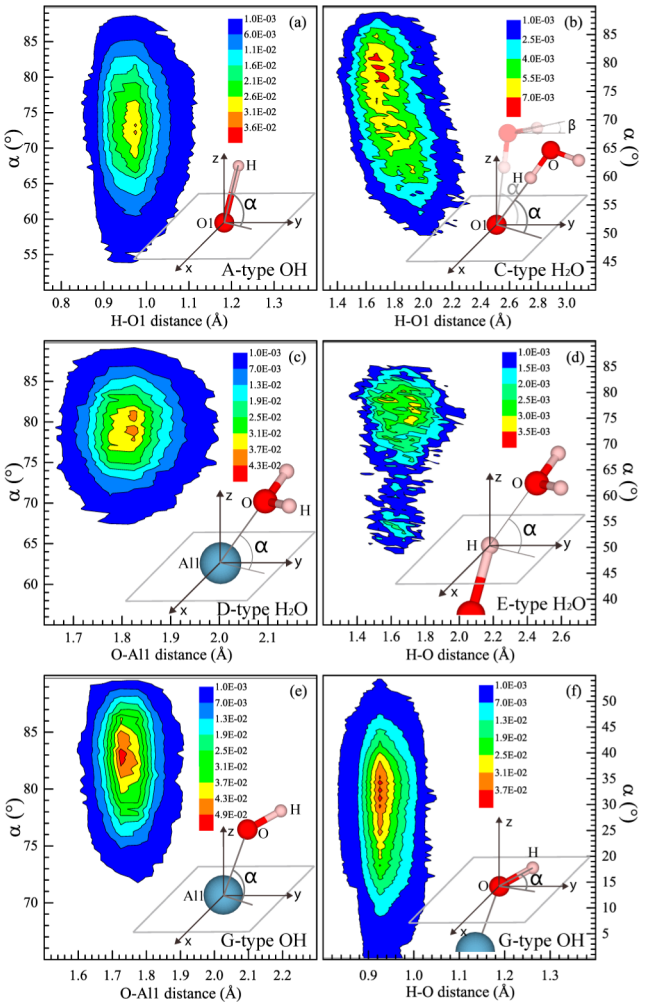

Figure 3. Distributions of bond length and the corresponding deviation angle α for various configurations: (a) the adsorption of dissociated H atom on O1 site, A-type OH; (b) the adsorption of OH-downward water molecule on O1 site, C-type water; (c) the adsorption of OH-upward water molecule on Al1 site, D-type water; (d) the adsorption of OH-upward water molecule on A-type OH and E-type water; and (e and f) the adsorption of dissociated OH on Al1 site, G-type OH group.

main angle α of ~80° and the other one tilts upward with the angle β of ~5°. The angle β accordingly fluctuates in the range of ~−25−15° when the angle α swings in the range of ~50−90°. The C-type water is worthy of notice because its existence is the precondition of surface hydroxylation (water dissociation), e.g., producing the surface A-type OH. In Figure 4a, one can note that the spatial projection distributions of the A4 OH group superpose that of B4 H, which just corresponds to the process of surface hydroxylation during the simulation. More details about this reaction will be discussed in section F. The spatial projection distributions of these C-type water molecules are shown in Figure 4b (C1, C2, C3, C4, C5, and C6). Though B2 shown in Figure 4a also corresponds the H atom of water molecules having one OH group toward O1 site, the other OH group of this water molecules points to the interior of the adsorbed water film. In this instance, the orientation order parameter θ of this water molecule is less than 90°. We will discuss B2 projection in combination with the spatial projection distributions of other water molecules in the following paragraph.

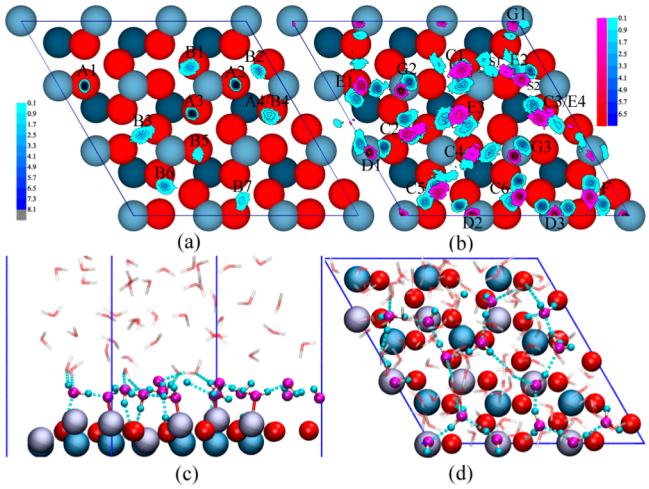

Figure 4. Spatial distribution of O (pink) and H (cyan) atoms of water projected on the Al-terminated α-Al_2O_3 (0001) surface and the snapshot of the contacting layer I. The red spheres represent the O atoms within O1 layer, while the light blue (dark blue) spheres represent the Al atoms within Al1 (Al2) layers. (a) The projection of H atoms within the range of 0−1.95 Å from the Al1 surface; (b) the projection of O and H atoms within the range of 1.15−3.35 Å from the Al1 surface; (c and d) the side and top snapshot of the contacting layer I, in which the HBs showed in cyan dashed lines. The letters from A to G denote various configurations of H atoms, OH groups, and water molecules, more details can be referred in the paper.

The third peak of H number density profile shown in Figure 2b results mainly from the H atoms of OH-upward water molecules. These OH-upward water molecules can be classified into two groups. In the first group, the OH-upward water molecules adsorbed atop the Al1 sites via O−Al1 interactions, the sketch of which is depicted and denoted as D-type water in Figure 3c. The spatial projection distributions of these D-type water molecules are shown in Figure 4b (D1, D2, and D3). The adsorptions of D-type water molecules atop Al1 sites arise from the low-coordination of the surface Al1 atoms, which provide strong Lewis acids sites for water adsorption. In these instances, the main distance between the O and the Al1 sites is ~1.8 Å, and the corresponding deviation angle α is mainly ~80°. In the second group, the OH-upward water molecules interacted with the A-type OH via HBs, as depicted and denoted by the character of E in Figure 3d. The distance between the O atom of E-type water and the H atom of A-type OH is mainly ~1.6 Å (HB length), and the corresponding deviation angle α is mainly ~80°. The spatial projection distributions of these E-type water molecules are shown in Figure 4b (E1, E2, E3, and E4). As the indication of A4/B4 shown in Figure 4a, the spatial projection distribution denoted as C3/E4 in Figure 4b corresponds the dissociation process of H from C-type water molecule, in which C-type water captured one transferring proton and subsequently transformed into E-type water molecule. Additionally, it can also be found that the spatial projection distribution of the E2 water molecule nearly superposes the projection of the surface A2 OH. In this instance, we observed that the E2 water molecule initially interacted with the surface A2 OH at S1 site, it then shifted to S2 site and one OH group of its tilted downward neighbor surface O1 site simultaneously, thereby resulting in the B2 projection shown in Figure 4a. When the E2 water molecule shifted from the S1 to S2 site, the variation of H−O distance is not evident, but the corresponding deviation angle α decreased much, from ~80 to ~55°, as shown in Figure

DOI: 10.1021/acs.jpcc.5b10695
J. Phys. Chem. C 2016, 120, 5398−5409

3d. In Figure 3d, the extension of contour shown from higle-angle and thick region to low-angle and thin region partly represents this displacement process. Though the D- and E-type water molecules adsorbed on Al1 and A-type OH sites via O atoms, respectively, the discrepancies of their adsorption sites resulted in their different orientation order parameters, θ. The D-type water molecule mainly preferred to be in OH-upward orientation, with the angle θ of ~50°, while the E-type water molecule tended to be parallel to the substrate, with the angle θ of ~80°.

We also showed the spatial projection distributions of water adsorption denoted as F and G (G1, G2, and G3) in Figure 4b. The F projections corresponds the water molecule with two OH groups almost paralleling to the surface, which is ~3 Å far from the Al1 layer. The G projections actually correspond the OH groups adsorbed on Al1 site, which stem from the dissociation of D-type water molecules due to water dissociation. The sketch of the G-type OH is shown in Figure 3e. The distance of O−Al1 is ~1.7 Å and the corresponding deviation angle α is ~82°. The bond length of the G-type OH is mainly ~0.93 Å, stretching in the range of ~0.83−1.03 Å, while its inclination angle is mainly ~30°, as indicated in Figure 3f. It can be noticed that the bond length of the G-type OH is shorter about 0.04 Å than that of the A-type OH. The orientation directions of the A- and G-type OH are also quite different. These differences arise from the higher coordination of O1 sites for A-type OH in comparison with that of G-type OH and bring about their different vibrational spectra. The ensemble average surface OH is ~6.38 per surface, ~0.71 ML coverage. Additionally, though the spatial projection of the G1 OH shown in Figure 4b looks like that of the D-type water molecule, it actually corresponds the direction turning of the G-type OH during the simulation.

As the above discussions, one can see that the structure of water layer I is complex, in which various adsorption states, such as the C-, D-, and E-type molecularly adsorbed water molecules and the A- and G-type surface OH, coexist. This complex structure accounts for the strong peak of the mass density profile shown in Figure 2a. Based on the DFT static calculations, Ranea et al. suggested that the water adsorption atop Al site competes with an alternative configuration of water bound to surface O through H with increasing coverage, which finally generate a hexagonal, ice-like layer up to 2 ML coverage, the adsorption energy of which was ~0.87 eV per water molecule.[15] However, the DFT calculations of Thissen et al. demonstrated that the Al-terminated surface favors the complex and hexagonal structures consisting of both dissociated and intact water monomers by forming HBs between preadsorbed H/OH groups and intact H_2O monomers with increasing the water coverage,[17] and the adsorption energy for the thin film is ~1.2 eV per water molecule. In Figure 4c,d, we show the snapshot of water layer I. One can see that the contacting layer I is well-defined, consisting of alternating dissociative water and molecularly adsorbed water monomers due to HBs bonding, the water coverage of which is approximately up to ~1.4 ML. This peculiar structure leads to the "ice-like" character, as we will show in section G about vibrational spectra.

F. Cooperative Dissociation of Interfacial Water Molecules. Five water dissociation (surface hydroxylation) reactions and one surface dehydroxylation reaction were observed in our simulations, which all are closely related to the cooperative dissociation through proton transferring. These reactions were very quick and completed within ~130 fs. Two comparable dissociation states, 1−4 and 1−4′ states, were observed (the 1−4′ state is sketched in Figure 5.). The 1−4

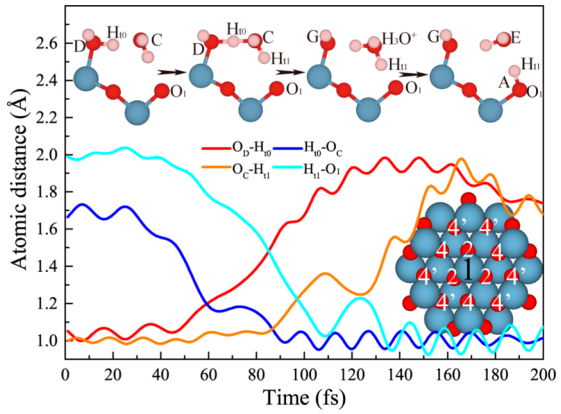

Figure 5. Schematic illustration of the indirect water dissociation to the 1−4′ state and the distance of the involved atoms with time evolution. The time axis is referred to any time before the occurrence of water dissociation. The top-view of the 1−2, 1−4, and 1−4′ dissociation states is depicted in the right-bottom inset.

dissociation process had been demonstrated in the work of Hass et al.[16] at lower and 1 ML coverage and other study[20] in detail. However, to our knowledge, the 1−4′ dissociation state has not been reported on the defective free Al-terminated α-$Al_2O_3(0001)$ surface.

In our simulations, the water dissociations to the 1−4′ state can be classified into two distinct types according to their different dissociation pathways. The first dissociation pathway, which is termed as indirect 1−4′ dissociation, was illustrated in Figure 5, as well as the distances of the involved atoms with time evolution. As shown in Figure 5, two neighboring water molecules, D- and C-type water molecules, were initially atop Al1 and O1 sites, respectively. As time evolution, the first transferring proton H^+_{t0}, which was originally bound to the O_D atom (O_X, the O atom of X-type water), shifted along the HB between O_D and O_C atoms and merged with the C-type water into the intermediate structure of H_3O^+ when D- and C-type water molecules approached each other, leaving D-type water transforming into G-type OH simultaneously. During this process, the O_D−H_{t0} distance increased from ~1.05 to ~1.9 Å, while the H_{t0}-O_C decreased from ~1.7 to ~1.0 Å. The intermediate H_3O^+ was ephemeral. The second transferring proton H^+_{t1} broke from the downward OH group of the H_3O^+ and subsequently adsorbed atop the O1 site once the transferring of H^+_{t0} was completed, and thereby the H_3O^+ transformed into the E-type water simultaneously. In this indirect 1−4′ dissociation, the proton indirectly transferred from D-type water to A-type OH (from 1 to 4′ site), assisted by the molecularly preadsorbed C-type water. Finally, two different G- and A-type surface OH and E-type water were produced.

The second dissociation pathway, which is termed as the double indirect 1−4′ dissociation, is illustrated in Figure 6. In the double indirect 1−4′ dissociation, the proton from D-type water to A-type OH was double indirectly assisted by a third neighboring water molecule and C-type water. As shown in Figure 6, two neighboring water molecules, the D- and C-type water molecularly adsorbed atop Al1 and O1 sites, respectively. As time evolution, the proton H^+_{t0} from D-type water molecule transferred to the third neighboring water molecule and formed

DOI: 10.1021/acs.jpcc.5b10695
J. Phys. Chem. C 2016, 120, 5398−5409

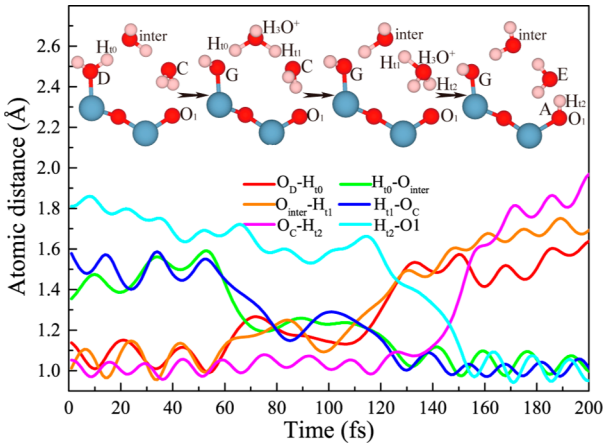

Figure 6. Schematic illustration of the double indirect water dissociation to the 1−4′ state and the distance of the involved atoms with time evolution. The time axis is referred to any time before the occurrence of water dissociation.

into the first intermediate structure of H_3O^+. During this process, the bond length of O_D−H_{t0} and H_{t0}−O_{inter} (O_{inter}, the O atom of the first intermediate water) fluctuated around the value of ∼1.1 and ∼1.5 Å, respectively. At the same time, the bond length of O_{inter}−H_{t1} was elongated from ∼1.05 to ∼1.2 Å due to H^+_{t0} approaching, which resulted in the reduction of H_{t1}−O_C bond length, from ∼1.5 to ∼1.2 Å. Subsequently, the proton H^+_{t1} of the H_3O^+ synchronically transferred to the *C*-type water when the H^+_{t0} merged into the intermediate water. Thus, the *C*-type water molecule also transformed into the second intermediate H_3O^+. Finally, the proton H^+_{t2} dissociated from the second intermediate H_3O^+ and bonded with O1 atom, leaving the second intermediate H_3O^+ transforming into the E-type water. This dissociation process also produced the G- and A-type surface OH. It is evident that the double indirect 1−4′ dissociation cannot occur at the low or monolayer water coverage because of its requirement of the two intermediate water molecules, thereby it is expected in many systems containing multiple water. The proton transferring occurred in the double indirect 1−4′ dissociation is identical to the "Grotthus mechanism", in which the excess proton transfers from one site to another site through water molecules.[54] Assisted by the peculiar configuration of step edge and lower terrace, the similar proton transferring was also reported at the H_2O/γ-AlOOH (Boehmite) (101) interface in a very recent theoretical study.[55]

As far as the five reactions of water dissociations, two reactions occurring at ∼2.4 and ∼21.5 ps followed the 1−4 pathway, one reaction occurring at ∼1.2 ps followed the indirect 1−4′ pathway, and two reactions occurring at ∼2.6 and ∼56.9 ps followed the double indirect 1−4′ pathway. Though it is hard to directly obtain the free energy barriers for the 1−4 and 1−4′ dissociation pathways in our simulations, we can approximately estimate these values with transition state theory. In transition state theory, the reaction rate k can be obtained with the expression, $k = (k_BT/h)\exp(-\Delta F/k_BT)$, where k_B, T, h, and ΔF are Boltzmanns' constant, temperature, Planck's constant, and the free energy barrier, respectively. Two 1−4 dissociation reactions occurred within ∼22 ps, the reaction rate of which can be estimated to be $k_{1-4} = \sim 0.091\ ps^{-1}$. Similarly, the reaction rate of 1−4′ is estimated to be $k_{1-4'} = \sim 0.053\ ps^{-1}$. Substituting the k_{1-4} and k_{1-4} to the above equation, the free energy barriers of 1−4 and 1−4′ dissociation were estimated to be ∼0.14 and ∼0.15 eV, respectively. Our estimated barrier of 1−4 dissociation is comparable with the value, ∼0.1 eV, obtained by constrained MD simulation[16] and static calculation[20] for single water dissociation. Therefore, the estimated barrier of 1−4′ dissociation, ∼0.15 eV, is acceptable. Though the reaction barrier can be lowered due to the cooperative dissociation assisted by proton transferring,[16] the barrier stepwise increased with the increasing hydroxyl coverage. It is reasoned that the time interval of contiguous reaction increases from ∼1 ps to ∼19 ps to 35 ps. Therefore, the barriers we obtained are more or less overestimated. As the inset showed at the right-bottom of Figure 5, one can find that the number of possible 1−4′ dissociation states is double that of the 1−4 states for D-type water atop 1 (Al1) site. It indicates that the 1−4′ dissociation pathway is slightly more favorable than 1−4 pathway under the condition of multiple water layer since the energy barriers of 1−4 and 1−4′ dissociate state are nearly equal, which is consistent with our observation. It should be noted that three of five reactions we observed occur at the initial stage of the simulation; thus, the proposed dissociation process might be affected by the initial configurations.

In addition, we also observed one surface dehydroxylation reaction of one H atom removal from the surface O1 site, which took place between the surface A-type OH and the neighboring G-type OH which exactly followed the inverse process of double indirect 1−4′ dissociation. Though the dehydroxylation reaction occurred, the surface dehydroxylation/hydroxylation ratio of 1/5 indicates that the surface hydroxylation is predominant in this stage.

G. Vibrational Spectra. Spectrum analysis of the O−H vibrational mode is one of the most widely used methods for characterizing the water adsorption on the alumina surface. Therefore, we estimated the vibrational spectra of the water film and of various water layers from layer I to layer VI, as shown in Figure 7. These vibrational spectra were calculated

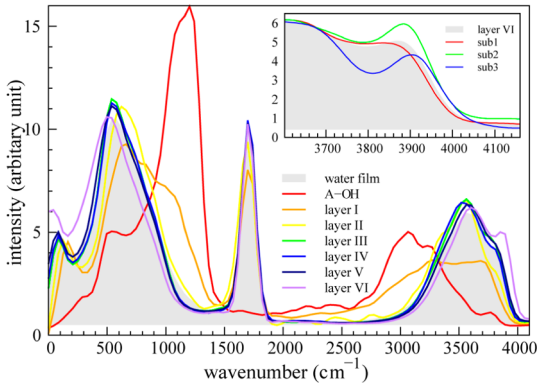

Figure 7. Computed vibrational spectra of water film and of various water layers from I to VI. The vibrational spectrum of surface A-type OH was also shown for comparison. The inset is the computed vibrational spectra of the water layer VI and its sublayers 1, 2, and 3.

from the appropriate D velocity−velocity autocorrelation functions, and the peak positions were rescaled by the factor of sqrt(2) to correct for the substitution of D for H.

The peaks positioned at ∼1690 cm^{-1} shown in Figure 7 correspond to the OH bending modes of water molecules, which are only present in the vibrational spectra of the whole water film and various water layers. Our calculated vibrational

DOI: 10.1021/acs.jpcc.5b10695
J. Phys. Chem. C 2016, 120, 5398−5409

frequency of the bending mode is consistent with the bulk liquid water value of ~1658 cm^{-1} using first-principles MD at 407 K,[56] and with the measured value of 1680 cm^{-1} at 353 K by attenuated total reflection (ATR) method.[57] The broad spectra at low frequency range (<1000 cm^{-1}) result from the hindered translational and librational motions of water molecules, which are beyond the scope of this work. Here, we mainly focused on the interpretation of the OH stretching modes in the range of 2500−4000 cm^{-1}. In this range, the peak of the water film positioned at ~3570 cm^{-1} corresponds the OH stretching mode of water molecules, which is also consistent with the measurement of 3550 cm^{-1}.[57]

In the range of 2500−4000 cm^{-1}, the distinct differences of the water layers are characterized by the blue- or red-shifting of the vibrational spectra in reference to that of the whole water film. The water layer V is bulk-like; therefore, its vibrational spectrum is almost identical to that of the water film. The spectrum outline of water layer VI is slightly different, and the blue-shifting of the vibrational spectrum can be noticed. The main OH stretching mode of water molecules in layer VI is at the position of ~3600 cm^{-1}, while another small peak appears at the position of ~3875 cm^{-1}. Further spectrum analysis indicated that the small peak is highly associated with the water molecules close to the water/vacuum interface. We divided layer VI into three sublayers according to the variation of the HBs number of per water molecule shown in Figure 2d, the ranges of which are ~18.3−20.9, ~20.9−22.6, and ~22.6−27.2 Å for sublayers 1, 2, and 3, respectively. We showed the vibrational spectra of the three sublayers in the inset of Figure 7. It is noticed that the small spectrum peak of layer VI results from the overlap of the spectra peaks of the sublayers 1, 2, and 3 positioned at ~3850, ~3880, and ~3905 cm^{-1}, respectively. These spectra peaks and their blue-shifting become pronounced as approaching the water/vacuum interface. The HB number of per water molecule dramatically decreases to 2.2 in sublayer 3, thereby the stretching vibration of the OH shifts to higher frequency. In contrast to water layer VI, though the spectra outlines of the water layer II, III, and IV are generally similar to that of the water film, but the red-shifting of these vibrational spectra were observed. The OH stretching modes of water molecules in layer II, III, and IV are shifted to the low frequencies of ~3550, ~3565, and 3535 cm^{-1}, respectively.

The vibrational spectrum of layer I is displayed in Figure 8a in detail, the spectrum outline of which is determined by the normalized fractional contributions of the surface A- and G-type OH, and of the molecularly adsorption water in various types of C, D, E, and F. To eliminate the uncertain interference on the spectrum calculations, only those OH group or water molecules which were not involved in water dissociations and proton transferring during the last 30 ps were considered. It is seen that the vibrational spectrum of layer I is very broad, and two approximately equal shoulders in intensity arise at the positions of ~3280 and ~3700 cm^{-1}. The broad spectrum of layer I is expected since it results from the spectra overlap of the dissociative A- and G-type OH groups and various molecularly adsorbed H_2O molecules, the fractional contributions of which are particularly discussed in the following discussions.

The vibrational spectrum of the surface OH is shown in Figure 8b, together with the contribution of A- (A1, A2, and A3) and G-type OH (G1, G2, and G3). It is seen that the main peak positioned at ~3670 cm^{-1} and the small hump positioned at ~3860 cm^{-1} result mainly from the stretching vibration of

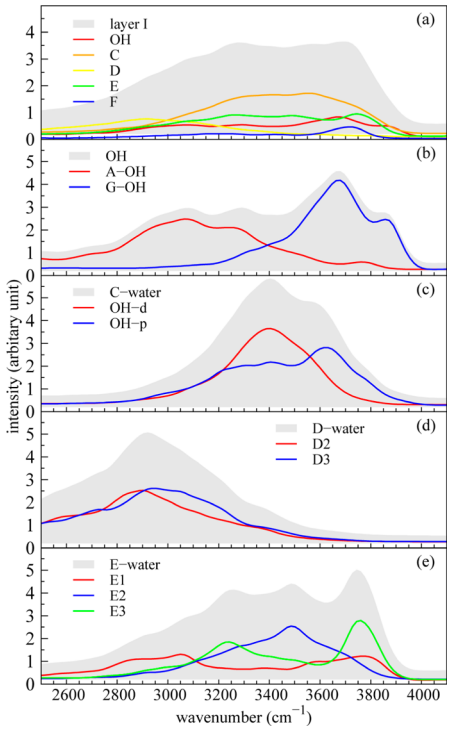

Figure 8. Computed vibrational spectra of layer I and the contributions (a) from the surface A- and G-type OH group (b) and from the specific molecularly adsorption waters, C- (c), D- (d), and E-type (e) water molecules. The intensity of individual contributions from the various states in (a) were normalized.

the G-type OH, while the two small peaks positioned at ~3075 and ~3290 cm^{-1} stem mainly from the stretching vibration of the A-type OH. In most times, the surface A-type OH groups played the role of the HB donor and interacted with E-type water molecules. Therefore, the stretching frequency of the A-type OH was lowered due to the constraint of the HB. Without this constraint, the vibrational frequency of A-type OH is ~3450 cm^{-1}.[16] The G-type OH, by contrast, which experienced less HBs interactions, shows a high frequency. Thus, the sharp feature commonly observed at the range of ~3700−3730 cm^{-1}[23,32,58] can be assigned to the G-type surface OH.

The C-type water molecularly adsorbed atop O1 sites via the downward OH (OH-d), and another OH which is almost parallel to Al1 surface (OH-p), as shown in Figure 3b. Therefore, two distinct peaks resulting from the two OH groups with different directions can be expected in their vibrational spectra. Only the C-type water of C1, C2, and C5 were considered in the spectrum calculation since the final configurations or the positions of C3, C4, and C6 change much in comparison with their initial states. Thus, the vibrational spectrum of the selected C-type water molecules displayed in Figure 8c is slightly different from that shown in Figure 8a. In Figure 8c, one can find that the peak at the position of ~3400 cm^{-1} stems mainly from the contribution of the stretching vibration of OH-d. This low frequency of OH-d indicates that its stretching mode is slightly restricted by the surface O1 atom via HB, while the higher frequency of OH-p at the position of ~3620 cm^{-1} imply that OH-p group experience less HBs restriction. Hass et al.[16] suggested that the commonly observe peak at ~3430 cm^{-1}[23,32] could come from the surface hydrogen-bonded OH groups (A-type OH). In the SFVS study of Zhang et al.,[32] it was found the intensity of ~3430

DOI: 10.1021/acs.jpcc.5b10695
J. Phys. Chem. C 2016, 120, 5398−5409

cm^{-1} decreased with surface drying, thereby they inferred this typical peak originates from the bonded OH stretches of adsorbed water. The vibrational spectrum shown in Figure 8c confirms that the typical frequency of ~3430 cm^{-1} observed by Zhang et al. stems from the stretching vibration of OH-d group of C-type water molecules.

In the spectrum calculation of D-type water, only the D2 and D3 water molecules were considered since the D1 water transformed into the G-type OH following the double indirect 1−4′ pathway. The stretching mode of D-type water is ~2920 cm^{-1} and red-shifted about 670 cm^{-1} in comparison with that of the water film, which may stem from the strong intermolecular coupling. As shown in Figure 4b,d, the two OH groups of D-type water molecules can readily bond with surrounding O atoms via HBs.

Further decomposition of the vibrational spectrum of the E-type water is shown in Figure 8e. In this instance, only the E-type water of E1, E2, and E3 were considered. It is seen that the spectrum of *E*-type water is broad and there are three small peaks positioned at ~3250, ~3490, and ~3750 cm^{-1}. These divergent stretching modes may result from that the three E-type waters atop A-type OH have a large degree of freedom to experience different HBs environments. In the study of a thin water film on a hydroxylated α-$Al_2O_3(0001)$ surface using FTIR spectroscopy, Thomas et al. observed the lower peak of ~3100 cm^{-1}.[24] They assigned it to the water molecules hydrogen-bonded with surface hydroxylated groups or interfacial water. The spectrum peak of E1 is ~3060 cm^{-1}, which can be comparable with their assignment. The E-type water, which hydrogen-bonded with A-type OH, is very similar to the water assigned by Thomas et al. The F-type water molecule is just at the boundary between layer I and II, in which instance it experiences few HBs and shows higher stretching frequency at the position of ~3720 cm^{-1}.

The two shoulders with lower and higher frequency of layer I displayed in Figure 8a is a bit similar to the shoulders commonly observed in a variety of experimental and theoretical studies of water/solid interface.[23,26−28,31−34,37] The observed shoulders with lower and higher frequency are close to the dominant spectra peaks observed on ice (~3100−3200 cm^{-1}) and liquid waters (~3550 cm^{-1}), respectively, thereby they are labeled as "ice-like" and "liquid-like" peaks correspondingly.[31−34] In our calculations, the shoulder with lower frequency of ~3280 cm^{-1} is also close to the dominant spectra peak observed on ice, the "ice-like" feature of which can be produced by overlapping multiple bands of different water states appeared in layer I, such as A-type OH, D-type and E1 H_2O molecules. The stretching modes of A-type OH, D-type and E1 H_2O molecules are highly restricted by its surrounding HBs. Therefore, it is evident that the "ice-like" peak arises from the stretching vibration of surface OH and water molecules that experienced more HBs interactions. It is reasonable to infer that the "ice-like" peak is the common character of the ordered hydration layer, since the formation of the ordered hydration layer is almost constructed with the HBs networking.

In Huang et al.'s study of water/hydroxylated α-Al_2O_3 (0001) interface,[37] two "ice-like" peaks (~3111 and ~3280 cm^{-1}) and one "liquid-like" (~3464 cm^{-1}) were identified. In their study, the thickness of the interfacial water is up to ~5 Å. As shown in Figure 9, both the characteristic peaks of "ice-like" at ~3300 cm^{-1} and of "liquid-like" at ~3560 cm^{-1} can be reproduced when we defined the interfacial water as the sum of layer I and II. In this instance, the thickness of the interfacial

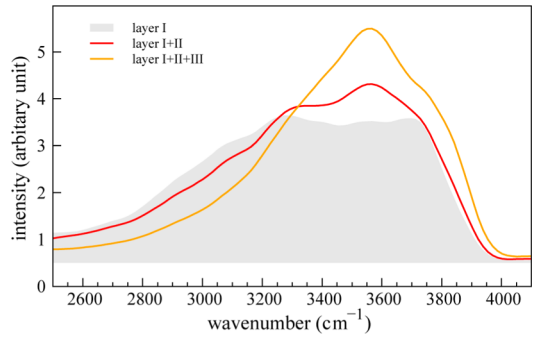

Figure 9. Computed vibrational spectra of the interfacial waters with different thickness.

water is ~5.1 Å and the contribution from "liquid-like" water molecules in layer II was included. However, if we only consider the layer *I* in our calculations, ~ 3.2 Å, the "OH-like" instead of "liquid-like" shoulder was observed at the higher frequency of ~3700 cm^{-1}. The "ice-like" peak almost disappears, and the intensity around 3550 cm^{-1} increases remarkably when the interfacial water was considered as the sum of layer I, II, and III. In most previous experiments, the "ice-like" and "liquid-like" shoulders were commonly observed under the hydorxylated surface conditions. Though the Al-terminated α-$Al_2O_3(0001)$ surface is used in our simulations, the "ice-like" and "liquid-like" shoulders were also reproduced with the interfacial water up to ~5.1 Å thickness. This result indicates that the appearance of the "ice-like" and "liquid-like" shoulders also exists in the water/Al-terminated α-$Al_2O_3(0001)$ interface. Furthermore, our results showed that the "ice-like" and "liquid-like" shoulders stem from the distinct interfacial water structure rather than the vibrational coupling between the stretching and bending overtone.

CONCLUSIONS

The structural properties and dynamical behaviors of the nanoscale water film adsorbed on the Al-terminated α-$Al_2O_3(0001)$ surface were investigated using the first-principles MD simulations, and the mechanism of surface hydroxylation/dehydroxylation process occurred at Al-terminated surface was uncovered. Furthermore, we calculated the vibrational spectra of specific water in various configurations within the contacting layer I and reproduced the "ice-like" and "liquid-like" shoulders observed in the water/hydroxylated α-$Al_2O_3(0001)$ interface.

Our simulations showed that the structural properties of the adsorbed water film, such as the mass density, atom number density, orientation order parameter and HBs of water molecules, are considerably affected by the presence of the Al-terminated α-$Al_2O_3(0001)$ surface along its normal direction. These properties are functioned with the distance from surface, and the properties of bulk liquid water recover beyond the distance of ~11 Å. The adsorbed water film can be divided into six distinct water layers according to its mass density variations. The higher mass density peak, which is up to ~4.30 g/cm^3, was noticed in layer I. Further examinations demonstrated that the higher mass density peak stems from the ordered hydration water layer consisting of C-, D-, and E-type water molecules, which is constructed via the HBs networking. Five water dissociation (surface hydroxylation) and one surface dehydroxylation reactions under the framework of cooperative proton transferring were observed in the whole simulation. A new dissociation 1−4′ state via two different indirect and

DOI: 10.1021/acs.jpcc.5b10695
J. Phys. Chem. C 2016, 120, 5398−5409

double indirect dissociation pathways is proposed. The estimated barrier of the 1−4′ dissociation pathway is ∼0.15 eV. The simulation showed that the 1−4′ dissociation pathway is slightly more favorable than the 1−4 pathway under the condition of multiple water layer. The C- and D-type water molecules can be considered as the "reactants" of these dissociation process, while the E-type water molecule and the A- and G-type OH group are the "products" in analogy. The surface dehydroxylation reaction just followed the inverse process of the 1−4′ double indirect dissociation pathway. The blue-shifting of layer VI and red-shifting of layer I, II, and III were noticed in our spectrum analysis, in reference to the bulk-like water layer V. The vibrational spectra of specific water in various configurations were calculated. It showed that the vibrational spectra of OH group and water molecules are dominated by their surrounding HBs. The "ice-like" and "liquid-like" peaks of vibrational spectra, which are commonly observed in various experiments of water/hydroxylated α-Al_2O_3(0001) interface, were reproduced under the condition of the Al-terminated α-Al_2O_3(0001) surface when the thickness of interfacial water is up to ∼5.1 Å. This result indicates that the appearance of the "ice-like" and "liquid-like" shoulders also exist in the water/Al-terminated α-Al_2O_3(0001) interface. Our calculations demonstrate that the "ice-like" peak is mostly ascribed to the A-type surface OH and the interfacial water molecules that experienced more HBs interactions in the ordered hydration layer, while the "liquid-like" peak stems from the vibrational modes of liquid-like water molecules.

AUTHOR INFORMATION

Corresponding Author

*Telephone: 86-10-56981827. E-mail: limin.liu@csrc.ac.cn.

Notes

The authors declare no competing financial interest.

ACKNOWLEDGMENTS

The authors wish to gratefully acknowledge financial support from the National Basic Research Program of China (No. 2011CB606403) and the National Natural Sciences Foundation of China (No. 51390470). The computational supports from the Informalization Construction Project of Chinese Academy of Sciences during the 11th Five-Year Plan Period (No.INFO-115-B01) and from the Beijing Computational Science Research Center (CSRC) are also highly acknowledged.

REFERENCES

(1) Hodgson, A.; Haq, S. Water Adsorption and the Wetting of Metal Surfaces. *Surf. Sci. Rep.* **2009**, *64*, 381−451.

(2) Feibelman, P. J. The First Wetting Layer on a Solid. *Phys. Today* **2010**, *63*, 34−39.

(3) Carrasco, J.; Hodgson, A.; Michaelides, A. A Molecular Perspective of Water at Metal Interfaces. *Nat. Mater.* **2012**, *11*, 667−674.

(4) Kelber, J. A. Alumina Surfaces and Interfaces under Non-Ultrahigh Vacuum Conditions. *Surf. Sci. Rep.* **2007**, *62*, 271−303.

(5) Henderson, M. A. The Interaction of Water with Solid Surfaces: Fundamental Aspects Revisited. *Surf. Sci. Rep.* **2002**, *46*, 1−308.

(6) Ahn, J.; Rabalais, J. W. Composition and Structure of the Al_2O_3 {0001}-(1 × 1) Surface. *Surf. Sci.* **1997**, *388*, 121−131.

(7) Eng, P. J.; Trainor, T. P.; Brown, G. E.; Waychunas, G. A.; Newville, M.; Sutton, S. R.; Rivers, M. L. Structure of the Hydrated α-Al_2O_3 (0001) Surface. *Science* **2000**, *288*, 1029−1033.

(8) Soares, E. A.; Van Hove, M. A.; Walters, C. F.; McCarty, K. F. Structure of the α-Al_2O_3(0001) Surface from Low-Energy Electron Diffraction: Al Termination and Evidence for Anomalously Large Thermal Vibrations. *Phys. Rev. B: Condens. Matter Mater. Phys.* **2002**, *65*, 195405.

(9) Di Felice, R.; Northrup, J. E. Theory of the Clean and Hydrogenated Al_2O_3(0001)-(1 × 1) Surfaces. *Phys. Rev. B: Condens. Matter Mater. Phys.* **1999**, *60*, R16287−R16290.

(10) Wang, X. G.; Chaka, A.; Scheffler, M. Effect of the Environment on α-Al_2O_3 (0001) Surface Structures. *Phys. Rev. Lett.* **2000**, *84*, 3650−3653.

(11) Liu, P.; Kendelewicz, T.; Brown, G. E.; Nelson, E. J.; Chambers, S. A. Reaction of Water Vapor with α-Al_2O_3(0001) and α-Fe_2O_3(0001) Surfaces: Synchrotron X-Ray Photoemission Studies and Thermodynamic Calculations. *Surf. Sci.* **1998**, *417*, 53−65.

(12) Elam, J. W.; Nelson, C. E.; Cameron, M. A.; Tolbert, M. A.; George, S. M. Adsorption of H_2O on a Single-Crystal α-Al_2O_3(0001) Surface. *J. Phys. Chem. B* **1998**, *102*, 7008−7015.

(13) Tzvetkov, G.; Zubavichus, Y.; Koller, G.; Schmidt, T.; Heske, C.; Umbach, E.; Grunze, M.; Ramsey, M. G.; Netzer, F. P. Growth of H_2O Layers on an Ultra-Thin Al_2O_3 Film: From Monomeric Species to Ice. *Surf. Sci.* **2003**, *543*, 131−140.

(14) Kelber, J. A.; Niu, C. Y.; Shepherd, K.; Jennison, D. R.; Bogicevic, A. Copper Wetting of α-Al_2O_3(0001): Theory and Experiment. *Surf. Sci.* **2000**, *446*, 76−88.

(15) Ranea, V. A.; Schneider, W. F.; Carmichael, I. DFT Characterization of Coverage Dependent Molecular Water Adsorption Modes on α-Al_2O_3(0001). *Surf. Sci.* **2008**, *602*, 268−275.

(16) Hass, K. C.; Schneider, W. F.; Curioni, A.; Andreoni, W. The Chemistry of Water on Alumina Surfaces: Reaction Dynamics from First Principles. *Science* **1998**, *282*, 265−268.

(17) Thissen, P.; Grundmeier, G.; Wippermann, S.; Schmidt, W. G. Water Adsorption on the α-Al_2O_3(0001) Surface. *Phys. Rev. B: Condens. Matter Mater. Phys.* **2009**, *80*, 245403.

(18) Wippermann, S.; Schmidt, W. G.; Thissen, P.; Grundmeier, G. Dissociative and Molecular Adsorption of Water on α-Al_2O_3(0001). *Phys. Status Solidi C* **2010**, *7*, 137−140.

(19) Ranea, V. A.; Carmichael, I.; Schneider, W. F. DFT Investigation of Intermediate Steps in the Hydrolysis of α-Al_2O_3(0001). *J. Phys. Chem. C* **2009**, *113*, 2149−2158.

(20) Wang, B. S.; Hou, H.; Luo, Y. B.; Li, Y.; Zhao, Y. M.; Li, X. L. Density Functional/All-Electron Basis Set Slab Model Calculations of the Adsorption/Dissociation Mechanisms of Water on α-Al_2O_3(0001) Surface. *J. Phys. Chem. C* **2011**, *115*, 13399−13411.

(21) Kirsch, H.; Wirth, J.; Tong, Y. J.; Wolf, M.; Saalfrank, P.; Campen, R. K. Experimental Characterization of Unimolecular Water Dissociative Adsorption on Alpha-Alumina. *J. Phys. Chem. C* **2014**, *118*, 13623−13630.

(22) Deng, X.; Herranz, T.; Weis, C.; Bluhm, H.; Salmeron, M. Adsorption of Water on Cu_2O and Al_2O_3 Thin Films. *J. Phys. Chem. C* **2008**, *112*, 9668−9672.

(23) Al-Abadleh, H. A.; Grassian, V. H. FT-IR Study of Water Adsorption on Aluminum Oxide Surfaces. *Langmuir* **2003**, *19*, 341−347.

(24) Thomas, A. C.; Richardson, H. H. Growth of Thin Film Water on α-Al_2O_3 (0001): An FTIR Study. *J. Phys. Chem. C* **2008**, *112*, 20033−20037.

(25) Florsheimer, M.; Kruse, K.; Polly, R.; Abdelmonem, A.; Schimmelpfennig, B.; Klenze, R.; Fanghanel, T. Hydration of Mineral Surfaces Probed at the Molecular Level. *Langmuir* **2008**, *24*, 13434−13439.

(26) Yeganeh, M. S.; Dougal, S. M.; Pink, H. S. Vibrational Spectroscopy of Water at Liquid/Solid Interfaces: Crossing the Isoelectric Point of a Solid Surface. *Phys. Rev. Lett.* **1999**, *83*, 1179−1182.

(27) Sung, J. H.; Zhang, L. N.; Tian, C. S.; Shen, Y. R.; Waychunas, G. A. Effect of pH on the Water/α-Al_2O_3 ($1\bar{1}02$) Interface Structure Studied by Sum-Frequency Vibrational Spectroscopy. *J. Phys. Chem. C* **2011**, *115*, 13887−13893.

(28) Sovago, M.; Campen, R. K.; Wurpel, G. W. H.; Muller, M.; Bakker, H. J.; Bonn, M. Vibrational Response of Hydrogen-Bonded

DOI: 10.1021/acs.jpcc.5b10695
J. Phys. Chem. C 2016, 120, 5398−5409

Interfacial Water Is Dominated by Intramolecular Coupling. *Phys. Rev. Lett.* **2008**, *100*, 173901.
(29) Gan, Y.; Franks, G. V. High Resolution Afm Images of the Single-Crystal α-Al_2O_3(0001) Surface in Water. *J. Phys. Chem. B* **2005**, *109*, 12474−12479.
(30) Argyris, D.; Phan, A.; Striolo, A.; Ashby, P. D. Hydration Structure at the α-Al_2O_3 (0001) Surface: Insights from Experimental Atomic Force Spectroscopic Data and Atomistic Molecular Dynamics Simulations. *J. Phys. Chem. C* **2013**, *117*, 10433−10444.
(31) Wei, X.; Miranda, P. B.; Shen, Y. R. Surface Vibrational Spectroscopic Study of Surface Melting of Ice. *Phys. Rev. Lett.* **2001**, *86*, 1554−1557.
(32) Zhang, L.; Tian, C.; Waychunas, G. A.; Shen, Y. R. Structures and Charging of α-Alumina (0001)/Water Interfaces Studied by Sum-Frequency Vibrational Spectroscopy. *J. Am. Chem. Soc.* **2008**, *130*, 7686−7694.
(33) Ostroverkhov, V.; Waychunas, G. A.; Shen, Y. R. Vibrational Spectra of Water at Water/α-Quartz (0001) Interface. *Chem. Phys. Lett.* **2004**, *386*, 144−148.
(34) Anim-Danso, E.; Zhang, Y.; Alizadeh, A.; Dhinojwala, A. Freezing of Water Next to Solid Surfaces Probed by Infrared-Visible Sum Frequency Generation Spectroscopy. *J. Am. Chem. Soc.* **2013**, *135*, 2734−2740.
(35) Argyris, D.; Ho, T. A.; Cole, D. R.; Striolo, A. Molecular Dynamics Studies of Interfacial Water at the Alumina Surface. *J. Phys. Chem. C* **2011**, *115*, 2038−2046.
(36) Argyris, D.; Ashby, P. D.; Striolo, A. Structure and Orientation of Interfacial Water Determine Atomic Force Microscopy Results: Insights from Molecular Dynamics Simulations. *ACS Nano* **2011**, *5*, 2215−2223.
(37) Huang, P.; Pham, T. A.; Galli, G.; Schwegler, E. Alumina-(0001)/Water Interface: Structural Properties and Infrared Spectra from First-Principles Molecular Dynamics Simulations. *J. Phys. Chem. C* **2014**, *118*, 8944−8951.
(38) Janeček, J.; Netz, R. R.; Flörsheimer, M.; Klenze, R.; Schimmelpfennig, B.; Polly, R. Influence of Hydrogen Bonding on the Structure of the (001) Corundum−Water Interface. Density Functional Theory Calculations and Monte Carlo Simulations. *Langmuir* **2014**, *30*, 2722−2728.
(39) VandeVondele, J.; Krack, M.; Mohamed, F.; Parrinello, M.; Chassaing, T.; Hutter, J. Quickstep: Fast and Accurate Density Functional Calculations Using a Mixed Gaussian and Plane Waves Approach. *Comput. Phys. Commun.* **2005**, *167*, 103−128.
(40) Perdew, J. P.; Burke, K.; Ernzerhof, M. Generalized Gradient Approximation Made Simple. *Phys. Rev. Lett.* **1996**, *77*, 3865.
(41) Krack, M. Pseudopotentials for H to Kr Optimized for Gradient-Corrected Exchange-Correlation Functionals. *Theor. Chem. Acc.* **2005**, *114*, 145−152.
(42) Goedecker, S.; Teter, M.; Hutter, J. Separable Dual-Space Gaussian Pseudopotentials. *Phys. Rev. B: Condens. Matter Mater. Phys.* **1996**, *54*, 1703−1710.
(43) Hartwigsen, C.; Goedecker, S.; Hutter, J. Relativistic Separable Dual-Space Gaussian Pseudopotentials from H to Rn. *Phys. Rev. B: Condens. Matter Mater. Phys.* **1998**, *58*, 3641−3662.
(44) Grossman, J. C.; Schwegler, E.; Draeger, E. W.; Gygi, F.; Galli, G. Towards an Assessment of the Accuracy of Density Functional Theory for First Principles Simulations of Water. *J. Chem. Phys.* **2004**, *120*, 300−311.
(45) VandeVondele, J.; Mohamed, F.; Krack, M.; Hutter, J.; Sprik, M.; Parrinello, M. The Influence of Temperature and Density Functional Models in Ab Initio Molecular Dynamics Simulation of Liquid Water. *J. Chem. Phys.* **2005**, *122*, 014515−014516.
(46) Todorova, T.; Seitsonen, A. P.; Hutter, J.; Kuo, I. F. W.; Mundy, C. J. Molecular Dynamics Simulation of Liquid Water: Hybrid Density Functionals. *J. Phys. Chem. B* **2006**, *110*, 3685−3691.
(47) Catalano, J. G. Weak Interfacial Water Ordering on Isostructural Hematite and Corundum (001) Surfaces. *Geochim. Cosmochim. Acta* **2011**, *75*, 2062−2071.
(48) Liu, L.; Krack, M.; Michaelides, A. Density Oscillations in a Nanoscale Water Film on Salt: Insight from Ab Initio Molecular Dynamics. *J. Am. Chem. Soc.* **2008**, *130*, 8572−8573.
(49) Liu, L. M.; Krack, M.; Michaelides, A. Interfacial Water: A First Principles Molecular Dynamics Study of a Nanoscale Water Film on Salt. *J. Chem. Phys.* **2009**, *130*, 234702.
(50) Liu, L. M.; Zhang, C. J.; Thornton, G.; Michaelides, A. Structure and Dynamics of Liquid Water on Rutile TiO_2(110). *Phys. Rev. B: Condens. Matter Mater. Phys.* **2010**, *82*, 161415.
(51) Tocci, G.; Michaelides, A. Solvent-Induced Proton Hopping at a Water-Oxide Interface. *J. Phys. Chem. Lett.* **2014**, *5*, 474−480.
(52) Luzar, A.; Chandler, D. Effect of Environment on Hydrogen Bond Dynamics in Liquid Water. *Phys. Rev. Lett.* **1996**, *76*, 928−931.
(53) Luzar, A.; Chandler, D. Hydrogen-Bond Kinetics in Liquid Water. *Nature* **1996**, *379*, 55−57.
(54) Sadeghi, R. R.; Cheng, H. P. The Dynamics of Proton Transfer in a Water Chain. *J. Chem. Phys.* **1999**, *111*, 2086−2094.
(55) Motta, A.; Gaigeot, M. P.; Costa, D. Ab Initio Molecular Dynamics Study of the Alooh Boehmite/Water Interface: Role of Steps in Interfacial Grotthus Proton Transfers. *J. Phys. Chem. C* **2012**, *116*, 12514−12524.
(56) Zhang, C.; Donadio, D.; Galli, G. First-Principle Analysis of the Ir Stretching Band of Liquid Water. *J. Phys. Chem. Lett.* **2010**, *1*, 1398−1402.
(57) Maréchal, Y. The Molecular Structure of Liquid Water Delivered by Absorption Spectroscopy in the Whole Ir Region Completed with Thermodynamics Data. *J. Mol. Struct.* **2011**, *1004*, 146−155.
(58) Coustet, V.; Jupille, J. High-Resolution Electron-Energy-Loss Spectroscopy of Isolated Hydroxyl-Groups on α-Al_2O_3(0001). *Surf. Sci.* **1994**, *307*, 1161−1165.

DOI: 10.1021/acs.jpcc.5b10695
J. Phys. Chem. C 2016, 120, 5398−5409